



## ORIGINAL ARTICLE

# Ni(II)-selective PVC membrane sensor based on 1,2,4-triazole bis Schiff base ionophore: Synthesis, characterization and application for potentiometric titration of Ni<sup>2+</sup> ions against EDTA



Gharam I. Mohammed<sup>a,\*</sup>, Amr L. Saber<sup>a,b,\*</sup>, Hoda A. El-Ghamry<sup>a,c,\*</sup>,  
Jalal T. Althakafy<sup>a</sup>, Hussain Alessa<sup>a</sup>

<sup>a</sup> Chemistry Department, Faculty of Applied Science, Umm Al-Qura University, Makkah, Saudi Arabia

<sup>b</sup> Chemistry Department, Faculty of Science, Zagazig University, 44519 Zagazig, Egypt

<sup>c</sup> Chemistry Department, Faculty of Science, Tanta University, Tanta, Egypt

Received 30 March 2021; accepted 4 May 2021

Available online 11 May 2021

## KEYWORDS

1,2,4-triazole;  
Ionophore;  
Electrode;  
Membrane;  
Sensors;  
Schiff base ligand

**Abstract** This study involves the preparation and investigation of a novel and highly selective poly (vinyl chloride)-based membrane of 2-((5-(2-hydroxy-3-methoxybenzylideneamino)-2H-1,2,4-triazol-3-ylimino)methyl)-6-methoxyphenol Schiff base ligand (HMBT), which is a neutral ionophore with sodium tetraphenyl borate (STB) in the form of an excluder and *o*-nitrophenyloctyl ether (*o*-NPOE) in the form of solvent mediators (plasticizing) as a Ni(II)-selective electrode. The observation of optimal performance was done wherein the membrane was shown to have the HMBT–PVC–NPOE–STB composition of 4:32:63:1. It worked effectively across a broad range of concentration ( $1.0 \times 10^{-8}$  to  $1.0 \times 10^{-2}$  mol L<sup>-1</sup>). Meanwhile, the Nernstian slope was recorded as 29.3 mV per decade of activity between pH 3.0 and 8.0. The response time of this electrode was fast at 11 s which was used for a span of 100 days with sound reproducibility. According to the selectivity coefficients for trivalent, divalent, and monovalent cations, excellent selectivity was indicated for Ni(II) ions across a large number of citations, whereas no interference was caused by anions like PO<sub>4</sub><sup>3-</sup>, SO<sub>4</sub><sup>2-</sup> and Cl<sup>-</sup>. The proposed method in this study was applied successfully to determine Ni(II) content in different samples of water, obtaining suitable recoveries. Additionally, the probed sensor is utilized as indicator electrode when considering Ni<sup>2+</sup> ion potentiometric titration against EDTA. In addition, the chelate's geometry and structure of the complex formed between Ni<sup>2+</sup> ions and HMBT, abbreviated as HMBT–Ni<sub>2</sub>, was evaluated by separating the solid

\* Corresponding authors at: Chemistry Department, Faculty of Applied Science, Umm Al-Qura University, Makkah, Saudi Arabia.

E-mail addresses: [giabulkair@uqu.edu.sa](mailto:giabulkair@uqu.edu.sa) (G.I. Mohammed), [alhefny@uqu.edu.sa](mailto:alhefny@uqu.edu.sa) (A.L. Saber), [haelghamry@uqu.edu.sa](mailto:haelghamry@uqu.edu.sa) (H.A. El-Ghamry).

Peer review under responsibility of King Saud University.



Production and hosting by Elsevier

product. Complex structure was confirmed based on alternative analytical and spectral methods to be structured in the bimetallic form with the formula  $[\text{Ni}_2(\text{HMBT})(\text{H}_2\text{O})_2 \text{Cl}_2]$ . The diamagnetic nature of the complex, which was concluded from the room temperature magnetic moment measurement combined with the UV–Vis measurement, suggested the square planar geometry around the Ni centers.

© 2021 The Author(s). Published by Elsevier B.V. on behalf of King Saud University. This is an open access article under the CC BY-NC-ND license (<http://creativecommons.org/licenses/by-nc-nd/4.0/>).

## 1. Introduction

Alongside the fast improvement of industry, metal contamination has received an impressive consideration globally. Heavy metals can be effectively accumulated in human body due to their high solubility and most of them are known to be exceptionally poisonous (Chen et al., 2019). Nickel is considered as a fundamental minor component for man and it is the fifth most abundant component on Earth (Mattison et al., 2020). World Health Organization (WHO) and United States Environmental Protection Agency (USEPA) set up the greatest permissible measure of Ni in drinking water at 0.07 and 0.04 mg L<sup>-1</sup> (Aragay et al., 2011), respectively. As particulate matter, nickel contamination of the water is attributed to normal sources such as backwoods fires, volcanic outflows, windblown residue, and ocean salt splash - in addition to anthropogenic sources, which include the ignition of fuel oil, coal, and diesel (Mattison et al., 2020). Nickel is known to cause health problems such as hacking dermatitis, persistent bronchitis, dermatitis, cardiovascular and renal infections, and pneumonic fibrosis degeneration, among others (Jafarigol et al., 2021). Therefore, it is necessary to accurately determine metal ions in biological and environmental samples in order to investigate environmental pollution and public health issues (Chen et al., 2019; Jafarigol et al., 2021; Fan et al., 2016).

Given the widespread spread of nickel pollution in the environment, there is a need to employ new methods for monitoring and measuring nickel levels. Several methods including atomic absorption spectrometry (Huang et al., 1999; Gómez-Nieto et al., 2013; Dobrowolski and Otto, 2012; Arpa and Bektas, 2006; Minami et al., 2003; Meeravali and Kumar, 2012), Inductively coupled plasma, mass spectrometry and inductively coupled plasma – optical emission spectroscopy (ICP-MS and ICP-OES) (Martín-Cameán et al., 2014; Sereshti and Karimi, 2014), and ultraviolet – visible (UV–Vis) spectrophotometric methods (Qiao et al., 2012; Deng et al., 2013) have been utilized to quantify trace nickel in different samples. All these approaches have both pros and cons. However, there are some limitations such as the number of tin-intensive manipulation procedures, the need to take special training and use sophisticated instruments, or reduced sensitivity, therefore; rendering these methods are unsuitable to determine nickels (Li et al., 2006; Sun et al., 2006). Electrochemical methods are known to have widespread popularity due to instrumentation's availability, procedural simplicities, speed, precision and accuracy which makes them preferable for the determination of Ni.

Rapid determination of trace quantities of Ni<sup>++</sup> ion assumes great importance owing to its impact on human health. Potentiometric measurements based on ion-selective membrane electrodes (ISMEs) offer a number of advantages

such as fast response, easy preparation, wide linear dynamic range, simple procedures, relatively low detection limits, reasonable selectivity, low cost as well as application in turbid and colored solutions (Elmosallamy and Saber, 2016; Craggs et al., 1974). Several ion selective electrodes (ISEs) constructed primarily for alkaline earth/ alkali, some heavy and transition metal ions are now commercially available due to the extensive research in this area.

All of the previous facts and findings encourage us to synthesize the bis Schiff base ligand named 2-((5-(2-hydroxy-3-methoxybenzylideneamino)-2H-1,2,4-triazol-3-ylimino)methyl)-6-methoxyphenol (HMBT), and investigate its performance in poly(vinylchloride) (PVC) membranes based matrix which have been attempted (employed) for Ni(II)-selective sensors. A literature survey revealed that the reporting of selective electrodes of Ni(II) ion is rarely undertaken (Mashhadizadeh and Momeni, 2003; Mashhadizadeh et al., 2003; Gupta et al., 2000; Gupta et al., 1997; Mazloum et al., 2002; Gupta et al., 2007; Singh and Saxena, 2007; Gupta et al., 2008). Up to our knowledge, no attempt has been made with regard to HMBT as an ionophore, and o-NPOE to fabricate Ni(II) selective electrodes. For this reason, we attempted HMBT concerning Ni<sup>2+</sup> - selective sensors' fabrication through the use of various solvent mediators. A thorough study was conducted to evaluate different parameters that influence the membranes' response characteristics. The sensor's practical utility was proven via its usage to determine Ni<sup>2+</sup> in a real wastewater sample. A comparison of the data obtained by investigating membranes was done with the findings derived by complexometric cyanide ions titration. To better understanding the reaction taking place between the ionophore and Ni(II) ions, Ni(II) chelate of HMBT ligand was synthesized and characterized.

## 2. Experimental

### 2.1. Equipments and instruments

Structures of the ligand HMBT and its Ni complex have been confirmed using the following instruments and methods: Perkin-Elmer 2400 CHN elemental analyzer in the microanalytical center of Cairo University have been used for elemental analysis (% of C, H and N) whereas the metal content in Ni complex has been analyzed and determined inductive coupled plasma analysis with a PerkinElmer/Optima 7000 DV instrument. Molar conductivity (measured for 10<sup>-3</sup> M DMF of the complex) has been estimated at ambient temperature using Jenway conductivity meter. FTIR spectra of both ligand and its complex have been recorded using 1430-Perkin-Elmer infrared-spectrophotometer within 4000 to 400 cm<sup>-1</sup> range as KBr discs. Shimadzu spectrometer (model UV-3600) have been used to measure the UV–Vis spectra applying the nujol

mull technique. The magnetic susceptibility measurements of finally grinded metal complex have been measured using a Sherwood Scientific MK1-Model Gouy magnetic susceptibility balance. Thermogravimetric analysis (TGA) of perfectly dried ligand and Ni complex were recorded on TG-50-Schimadzu thermogravimetric analyzer under 10 °C/min heating rate and inert atmosphere inside the temperature ranging from ambient temperature up to 800 °C. Each of the potentiometric measurements was detected at room temperature ( $25 \pm 1$  °C) with a Hanna (HI2211-01) digital pH/mV meter using Ni-**HMBT**-PVC matrix membrane sensors with sensitivity of  $\pm 0.1$  mV combined with a double-junction Ag/AgCl reference electrode (Orion Model 90-02) that contained 10% (w/v) potassium nitrate in the outer compartment. The pH measurements were conducted using a 420A ionalyzer (Orion model) along with its glass electrode. The role of the ISE internal filling solution was served by a 0.01 mol L<sup>-1</sup> nickel (II) solution. (Ag/AgCl)/ internal solution (0.01 mol L<sup>-1</sup> nickel (II))/PVC membrane/sample solution/ (Ag/AgCl) reference electrode (Orion Model 90-02) carried out the all the aforementioned measurements.

## 2.2. Chemicals and solutions

Sodium tetraphenyl borate (STB), *o*-nitrophenyloctyl ether (o-NPOE) and high molecular mass poly (vinyl chloride) (PVC, 99%) were obtained from Fluka. Nickel(II) chloride hexahydrate, 3,5-diamino-1,2,4-triazole, *o*-vaniline, dioctyl phthalate (DOP), dioctylphenylphosphonate (DOPP), and bis(ethylhexyl)sebacate (DOS) and tetrahydrofuran (THF) were purchased from Aldrich. In order to prepare all aqueous solutions, doubly distilled water (DDW) was utilized.

## 2.3. Synthesis of ionophore (HMBT)

The ionophore bis Schiff base compound named 2-((5-(2-hydroxy-3-methoxybenzylideneamino)-2H-1,2,4-triazol-3-ylimino)methyl)-6-methoxyphenol (abbreviated as **HMBT**) has been synthesized by modification of a previously reported method (Chohan and Sumrra, 2010) in which 10 mmol of 1,2,4-triazole-3,5-diamine (0.99 g) dissolved in 20 ml hot ethanolic solution was dropped wisely and slowly added to boiled ethanolic solution containing 30 mmol of *o*-vaniline (1.52 g in 30 ml EtOH). The resulting reaction solution was left to reflux while stirring for 2 h during which orange yellow precipitate appeared. The reaction proceeded for another 2 h to ensure the reaction is complete. Finally, the formed product was obtained through filtration of the hot solution. The product was rinsed several times by using hot ethanol followed by ether and finally subjected to vacuum dryness over anhydrous CaCl<sub>2</sub>.

Yield: 2.84 g (77.4%). Colour: yellowish orange. m.p. 258 °C. Anal. Calcd (%) for **HMBT** (C<sub>18</sub>H<sub>17</sub>N<sub>5</sub>O<sub>4</sub>; 367.36 g mol<sup>-1</sup>): C, 58.85; H, 4.66; N, 19.06. Found: C, 58.87; H, 4.72; N, 19.08. EI-mass spectra  $m/z = 369$  (M+2). IR (cm<sup>-1</sup>, KBr phase): 3462(s), 3217(w), 1636(s), 1584(m), 1230(s), 1064(m).

## 2.4. Synthesis of complex Ni(II) complex (HMBT-Ni<sub>2</sub>)

Ni(II) complex of the ionophore bis Schiff base ligand **HMBT**, abbreviated as **HMBT-Ni<sub>2</sub>**, was synthesized by drop wise

addition of hot methanolic solution containing 0.476 g of NiCl<sub>2</sub>·6H<sub>2</sub>O (0.002 mol) in 10 ml MeOH to methanolic/DMF solution (90/10%) containing 0.367 g (0.001 mol) of **HMBT**. The resultant reaction solution was left to reflux with stirring for 2 h during which faint green precipitate was formed. The reaction extended for another 1 hour after which the precipitate was filtered from hot solution. The product was rinsed severally using hot ethanol followed by ether and finally subjected to vacuum dryness over anhydrous CaCl<sub>2</sub>.

Yield: 0.41 (69.6%). Colour: Faint green. m.p. 294 °C (chairing).  $\Lambda_m$  (Ω<sup>-1</sup> cm<sup>2</sup> mol<sup>-1</sup>) = 24.5. Anal. Calcd for **HMBT-Ni<sub>2</sub>** (C<sub>18</sub>H<sub>19</sub>N<sub>5</sub>Cl<sub>2</sub>O<sub>6</sub>Ni<sub>2</sub>; 589.67 g mol<sup>-1</sup>): C, 36.66; H, 3.25; N, 11.88; Ni, 19.91. Found: C, 36.71; H, 3.21; N, 11.91; Ni, 19.85. IR (cm<sup>-1</sup>, KBr phase): 3417(s, br), 3262(s, br), 1647(s), 1583(s), 1282(m), 1065(s), 597(w), 4533(w).

## 2.5. Preparation of electrode

The procedure for constructing PVC membranes involved mixing (32%) of powdered PVC and (4%) of ionophore **HMBT** with (63%) of plasticizers (o-NPOE, DOPP, DOP or DOS) as the solvent mediators and (1%) STB (Saber and Ahmed, 2016). This mixture was dissolved in 6 ml of THF by vigorous shaking and then poured into a glass ring with an inner diameter of 3 cm resting on a smooth glass plate. The evaporation of this solvent was done at 25 °C for 48 h. This was followed by the removal of the resulting membrane from the glass mold. Subsequently, disks whose diameter was 7 mm and average thickness was 0.2 mm were mounted on a laboratory-made electrode body (Saleh et al., 2001; Saber, 2010). To this mixture, an aqueous solution of 10<sup>-2</sup> M NiCl<sub>2</sub> was added as an internal reference solution amidst the presence of the electrode with a diameter of 1.0 mm. The involved electrodes were conditioned for a minimum of 48 h by soaking them in a fresh 0.01 M NiCl<sub>2</sub> solution in a dark place and subsequently storing it in the same solution.

## 2.6. Electrode calibration

Successive aliquots (20 ml) of 10<sup>-8</sup> and 10<sup>-2</sup> M of nickel chloride solutions were transferred into 50 ml beakers. Thereafter, all the Ni<sup>2+</sup> electrodes in conjunction with Ag/AgCl reference electrode were immersed inside the solution. After stirring, the stable electromotive force (e.m.f.) for each concentration was recorded and plotted as a function of the logarithm of nickel ion concentration. Linear working range and detection limit of the nickel electrode, the slope and unknown concentration of nickel ion solution were calculated from the resulting curve.

## 2.7. pH impact on the potential of electrode

A testing was done to determine the pH impact on the electrode potential measurements for 10<sup>-2</sup>, 10<sup>-3</sup> M of NiCl<sub>2</sub>. Then, 20 ml of all the solutions being tested were shifted to a 50 ml beaker followed by immersing the reference electrode (Ag/AgCl) along with the planned Ni(II)-selective electrode. This solution witnessed the immersion of a glass electrode system. The examined solutions' pH was found in the range of 2.0–10.0 by adding 0.1 M NaOH or 0.1 M HCl solutions.

## 2.8. Selectivity measurements

Another technique was used to determine the values of selectivity coefficient concerning chosen inorganic cations (IUPAC, 2000). This was done via a measurement of potential readings involving  $10^{-3}$  M of the interfering ion and  $10^{-3}$  M for  $\text{Ni}^{2+}$ . This was followed by a calculation of  $K_{\text{Ni}^{2+}}^{\text{pot}}$ , the selectivity coefficient. The following equation is used to calculate  $X^{Z+}$ .

$$\log K_{\text{Ni(II);XZ}^+}^{\text{pot}} = E_2 - E_1/S + \log[\text{Ni}^{2+}] - \log[X^{Z+}]^{1/Z}$$

where  $E_1$  denotes the electrode  $10^{-3}$  M of  $\text{Ni(II)}$  potential,  $E_2$  signifies the  $10^{-3}$  M solution's electrode potential of X, the interfering cation,  $S$  represents the calibration curve's slope at room temperature whereas  $Z$  denotes the interfering ion's charge.

## 2.9. Analytical application

### 2.9.1. Potentiometric titration

The practical utility of HMBT membrane sensor was examined by utilizing it as an indicator electrode. Titration of 10 ml of  $10^{-2}$  M  $\text{Ni}^{2+}$  solution was conducted against  $1 \times 10^{-2}$  M EDTA in the presence of pH 5 buffer solution (Welcher, 1958).

### 2.9.2. Water samples preparation

Filter paper (Whatman, No. 4) was used for disposing suspended particulate matter from the water samples (i.e., tap water and mineral water) by filtration and acidification using 5.0 ml of concentrated  $\text{HNO}_3$  before being stored inside polyethylene containers. Concentrated  $\text{NH}_3$  was utilized for neutralizing the solutions followed by adjusting pH to 5.0 with acetate buffer. This potentiometric procedure was carried out in compliance with the procedure laid out.

## 3. Results and discussion

### 3.1. Structure elucidation of HMBT and HMBT-Ni<sub>2</sub>

#### 3.1.1. Elemental analysis and general characteristics

Both HMBT and HMBT-Ni<sub>2</sub> compounds were separated and their compositions were confirmed by applying elemental analysis technique. The results supported the structure of HMBT to be as shown in Fig. 1 and the formation of its complex with Ni(II) ion in the bimetallic form. The molar conductivity of HMBT-Ni<sub>2</sub>, measured from  $10^{-3}$  M solution in DMF solvent, was calculated to be  $24 \Omega^{-1} \text{cm}^2 \text{mol}^{-1}$ . Such low value ensured the formation of the complex in the neutral form (saad et al., 2017; Gaber et al., 2019). The analytical results also supported the formula of the HMBT-Ni<sub>2</sub> as  $[\text{Ni}_2(\text{HMBT})(\text{H}_2\text{O})_2 \text{Cl}_2]$ . Both compounds are easily soluble in most polar solvents but barely soluble in alternative non-polar solvents. High purity of both compounds was confirmed through the sharpness melting point.

#### 3.1.2. Mass spectrum

The formation of HMBT ligand is represented in Fig. 1 and confirmed by the measurement of the mass spectrum

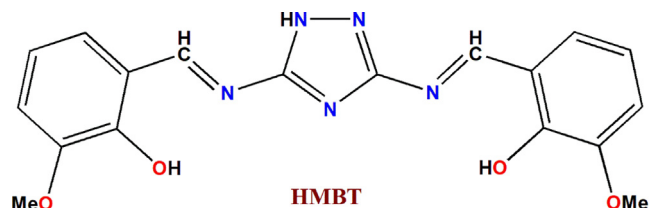


Fig. 1 Structure of HMBT ionophore.

(Fig. 2). According to Fig. 2, the base and molecular ion peak appearing at  $m/z$  369 corresponded to the  $(M+2)$  of HMBT (calculated molecular weight for HMBT with molecular formula of  $\text{C}_{18}\text{H}_{17}\text{N}_5\text{O}_4$  is 367.36). The peaks appearing at  $m/z$  352, 305, 276, 199, 171 and 101 were imputed to the various fragments as presented in Scheme 1. Almost all these fragments confirm the formation of the bis-Schiff base product.

#### 3.1.3. FTIR spectrum

Comparison of the spectrum of HMBT-Ni<sub>2</sub> with that of HMBT ligand is beneficial to assign the binding function groups of the ligand to the nickel center. Fig. 3 shows the IR spectra of both HMBT and HMBT-Ni<sub>2</sub>. The spectrum of HMBT illustrated the bands located at 3462, 3217, 1636, 1584, 1230,  $1064 \text{cm}^{-1}$  imputed to the stretching wavenumbers of OH, NH, C=N(imine), C=N(triazole ring), C=O and N=N bonds, respectively. A comprehensive study of the IR spectrum of HMBT-Ni<sub>2</sub> illustrated the existence of spectral peaks at 3417, 3262, 1647, 1583, 1282,  $1065 \text{cm}^{-1}$  (Chohan and Sumrra, 2010; Sumrra and Chohan, 2013). The bands located 1647 and 1282 were assigned to the stretching frequency of C=N(imine) and C=O, successively (Elsherbiny and El-Ghamry, 2015). These two bands exhibited a change in their places when compared with their places in the ligand spectra which confirms their connection to the Ni centers through N and O atoms, respectively. The bands appearing at 3417 and  $3262 \text{cm}^{-1}$  assigned to  $\nu(\text{OH})$  of water molecules connected to the metal center and  $\nu(\text{NH})$ , respectively (Saad et al., 2019). The position of the other groups; NH, C=N (triazole ring), and N=N bonds, did not show significant change in their places appearing almost at the same places as in the spectrum of HMBT and hence confirming that these groups did not participate in the complex formation. Further proof for the involvement of C=N and deprotonated OH in the complex formation is the generation of two new bands in the spectrum of HMBT-Ni<sub>2</sub> only with no equivalent peaks in the

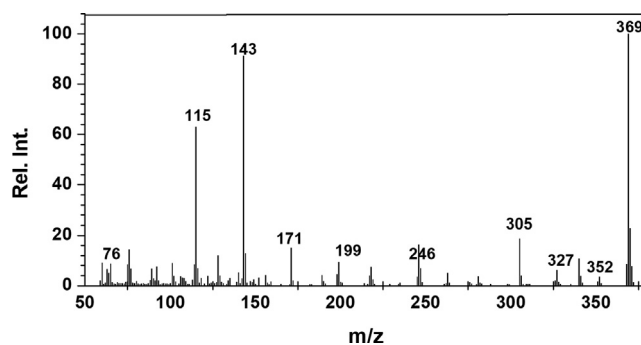
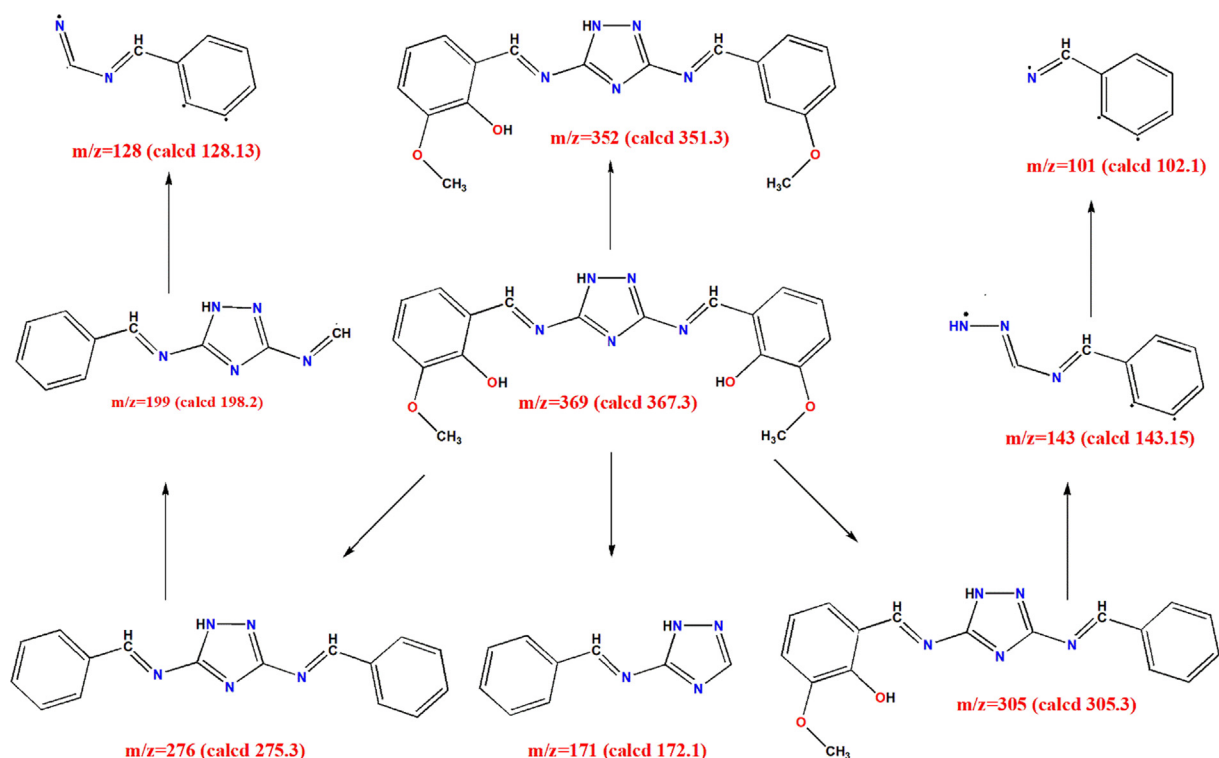
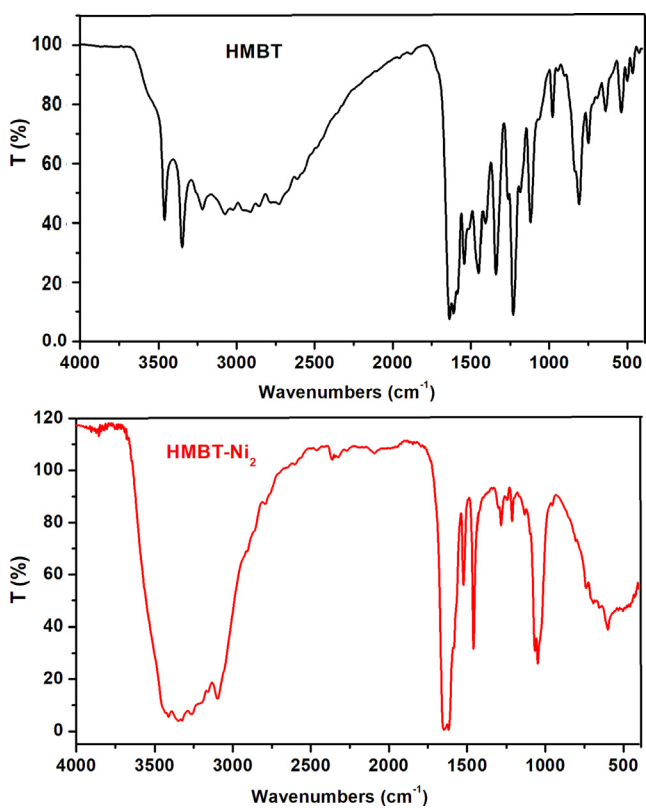


Fig. 2 Mass spectrum of HMBT ionophore.



**Scheme 1** Fragmentation pathways of HMBT indicating the calculated and found fragments molecular weights.



**Fig. 3** Representation of IR spectra of HMBT and its Ni(II) chelate, HMBT-Ni<sub>2</sub>.

spectrum of HMBT. The first band appeared at 597 and assigned to  $\nu(\text{Ni}-\text{O})$  whereas the second band appeared at 453 cm<sup>-1</sup> and assigned to  $\nu(\text{Ni}-\text{N})$ .

#### 3.1.4. Thermal analysis (TG/DTG) results

The analytical thermogravimetry (TG) is considered an important tool in structure elucidation through interpretation of temperature ranges of each decomposition step, types of intermediates and the final remnant left behind after the compounds are fully decomposed. Additionally, for coordination compounds, such analytical tool can also provide important knowledge concerning the solvent and anion molecules existing outside or inside the coordination sphere as a part of the complex structure. Accordingly, the TG thermogram and its first derivative (DTG) for HMBT and its Ni(II) chelate HMBT-Ni<sub>2</sub> are illustrated in Fig. 4.

From these thermograms, it is obvious that HMBT and HMBT-Ni<sub>2</sub> underwent full decomposition within the temperature range 25–800 °C through three and four decomposition stages, respectively, according to the following Schemes:

For HMBT, the first step appeared assigned to the loss of two methyl groups and the second step corresponded to the loss of triazole moiety in addition to half oxygen molecule. The last step assigned to the loss of the remaining part.

The four stages of HMBT-Ni<sub>2</sub> complex assigned to the loss of two coordinated water molecules within the first step and two methyl groups during the second step. The third corresponded to the loss of chlorine molecule and hydroxy phenyl group. The remaining organic ligand was forfeited within the fourth and last step of HMBT-Ni<sub>2</sub> decomposition resulting in the formation of the thermally stable NiO as a remnant pro-

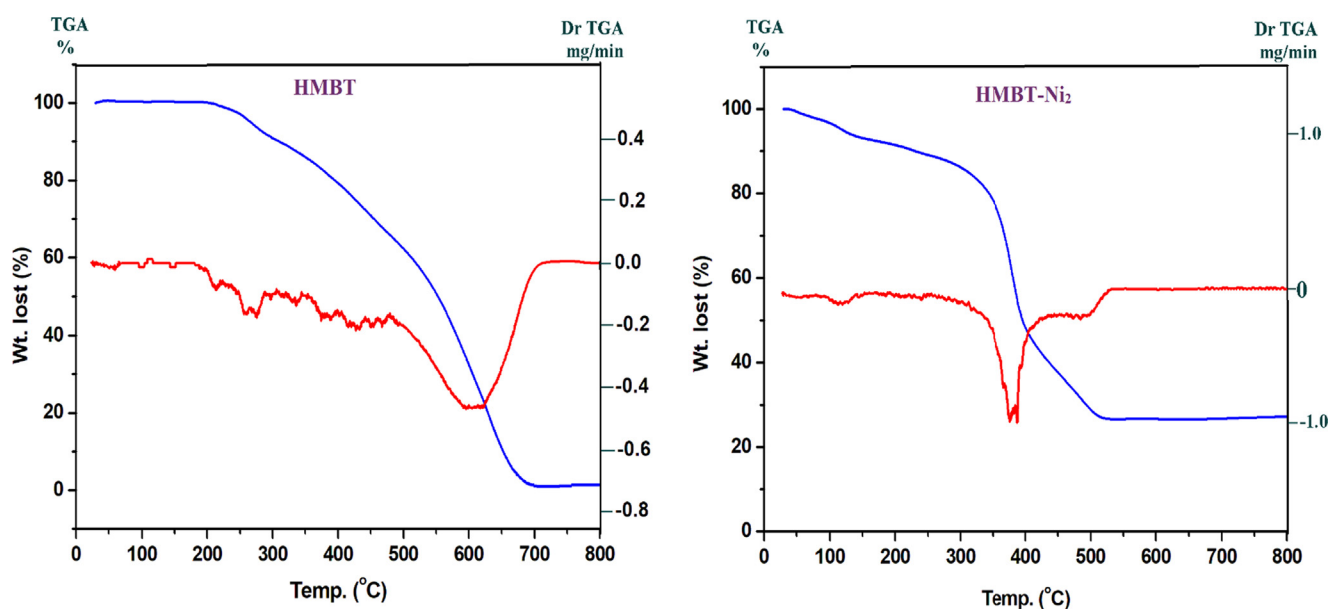


Fig. 4 TG/DTG thermograms of HMBT and its Ni(II) chelate, HMBT-Ni<sub>2</sub>.

duct from with the metal content in the complex has been estimated to be 20.21% which is close to the calculated percent.

### 3.1.5. UV-Vis spectra and magnetic moment inspection

The nujel mull spectrum of HMBT-Ni<sub>2</sub> represents the existence of three spectral bands with high to moderate intensities centered at 245, 312 and 395 cm<sup>-1</sup> (Fig. 5). The first two bands have inter-ligand charge transfer character. The band centered at 395 cm<sup>-1</sup> is characterized by having mixed inter-ligand charge transfer and ligand to metal charge transfer character (Kundu et al., 2015). The characteristic weak low energy and broad d-d bands centered around 636 cm<sup>-1</sup> which can be accounted by a square planar geometry for Ni(II) complexes in agreement with the compound diamagnetism (Kundu et al., 2015; Ibrahim et al., 2018).

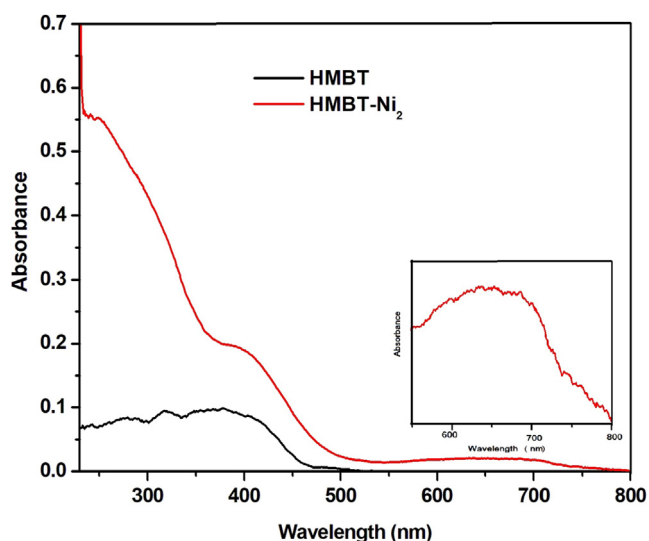


Fig. 5 UV-Vis spectra of HMBT and HMBT-Ni<sub>2</sub>.

### 3.1.6. Molecular modeling studies

The optimization of HMBT-Ni<sub>2</sub> structure was done using PM3 method implemented in HyperChem 8.0 program (HyperChem, 2007) to confirm the best geometrical arrangement of the ligand molecule around the Ni(II). The optimized structure of HMBT-Ni<sub>2</sub> due to the difficulty to get crystal structure. The optimized molecular structures of HMBT-Ni<sub>2</sub> are presented in Fig. 6. Table 1 represented some chosen bond distances and angles. From Fig. 6 and the data depicted in table 1, it is obvious that the nickel ions are positioned almost nearly in average flat plane delineated by the O and N donor atoms of the HMBT in addition to chloride ion and coordinated water oxygen atom. The cis angles around the Ni centers range from 87.00° to 99.72° approaching to the right angle. On the other hand, the trans angles, the smallest one is 170.16° and the largest is 174.41°, which are also the straight angle. Such angles ranges recommend marginally distorted square planar

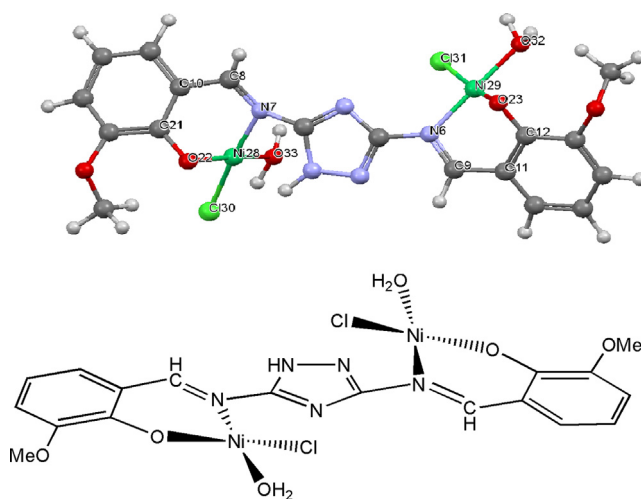


Fig. 6 The optimized and molecular structures of HMBT-Ni<sub>2</sub>.

**Table 1** Some chosen bond lengths (Å) and angles (°) of HMBT-Ni<sub>2</sub>.

Bond type	(Å)	Angle type	(°)
C11-C12	1.4467	H38-C27-H39	106.27
C12-O23	1.3145	N7-Ni28-O22	90.21
O23-Ni29	1.7955	N7-Ni28-Cl30	170.06
Ni29-O32	1.8766	O22-Ni28-Cl30	99.72
C4-N5	1.3611	O22-Ni28-O33	172.19
C4-N7	1.3855	N6-Ni29-Cl31	89.02
N6-C9	1.3025	O23-Ni29-O32	89
N6-Ni29	1.8696	Ni29-O32-H34	114.05
N7-C8	1.3055	Ni29-O32-H35	111.05
N7-Ni28	1.8163	Ni28-O33-H36	99.27

architecture around the Ni ions with almost no tetrahedral distortion (Ibrahim et al., 2018). Such distortion from the regular square planar structure is due to different character of the atoms forming the environment around the Ni(II) ions (Leovac et al., 2007).

### 3.2. Performance characteristics of sensors

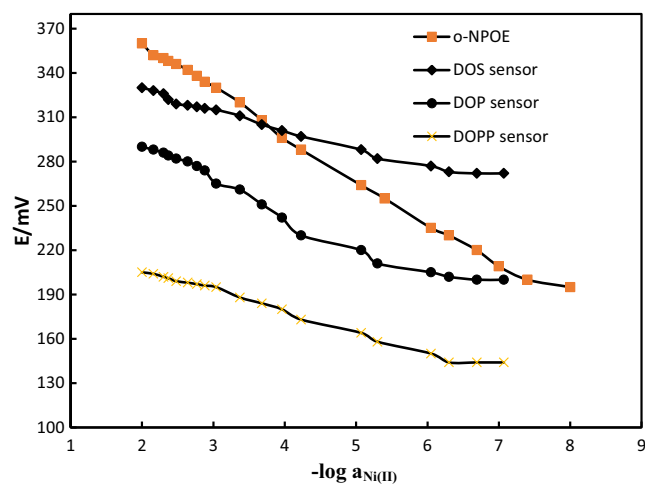
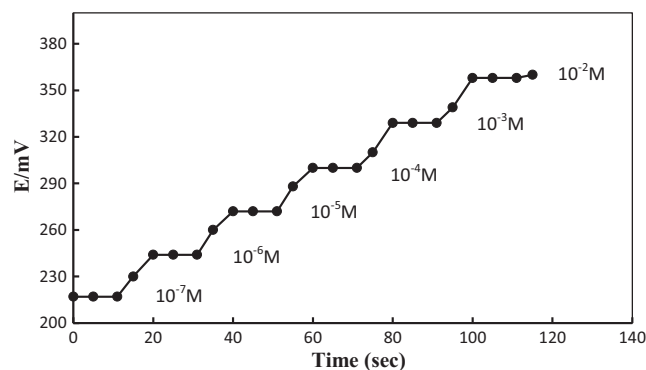
Four membrane compositions were investigated (Table 2). The statistical deviation data of slopes show that the preparation process is highly reproducible. Table 2 summarizes the response attributes of the fabricated selective electrodes of nickel ion. For each of these sensors, an evaluation of characteristics related to performance clearly demonstrated that the performance of sensors 1 membrane with *o*-NOPE plasticizer is optimal. The electrochemical behavior (Table 3) of the investigated sensor was examined in accordance with IUPAC recommendations (IUPAC, 2000). The sensor is known to show the widest working concentration range of  $1 \times 10^{-2} - 1 \times 10^{-8}$  M (Fig. 7), a Nernstian slope of  $29.3 \pm 0.2$  mV/decade for electrode with membrane 1. Meanwhile, the proposed sensor's minimum response time was shown to be 11 s (Fig. 8) by changing the Ni(II) concentration in a series of solutions ( $1.0 \times 10^{-2}$  to  $1.0 \times 10^{-7}$  mol l<sup>-1</sup>). Such sensor gave detection limit of  $5.0 \times 10^{-8}$  M. Thus, cells that employed sensor 1 were used for all additional studies.

### 3.3. Solvent mediators

It is important for plasticizers to maintain compatibility with polymers for ensuring feasible mechanical attributes. This

**Table 3** Response characteristics of Ni- HMBT -PVC membrane sensor.

Parameter	<i>o</i> -NPOE
Slope, (mV decade <sup>-1</sup> )	29.3
Intercept, (mV)	416.7
Correlation coefficient, (r)	0.9954
Lower limit of detection, (M)	$5.0 \times 10^{-8}$
Lower limit of linear range, (M)	$1.0 \times 10^{-7}$
Working pH range	3.0–8.0
Life span/days	100

**Fig. 7** Calibration curve of the Ni(II) membrane sensors.**Fig. 8** Dynamic response time of the electrode for step changes in the concentration of Ni(II).**Table 2** Response characteristics of nickel membranes based on HMBT and different solvent mediators.

Electrode no.	Ionophore	Solvent mediator	Slope (mV/decade)	Linear range (M)	Detection limit (M)	R.S.D. (%) (n = 3)
Type 1	HMBT	<i>o</i> -NPOE	29	$10^{-2} - 10^{-7}$	$5 \times 10^{-8}$	1.54
Type 2	HMBT	DOPP	13	$10^{-2} - 10^{-7}$	Undetected	–
Type 3	HMBT	DOP	20	$10^{-2} - 10^{-7}$	Undetected	–
Type 4	HMBT	DOS	12	$10^{-2} - 10^{-7}$	Undetected	–

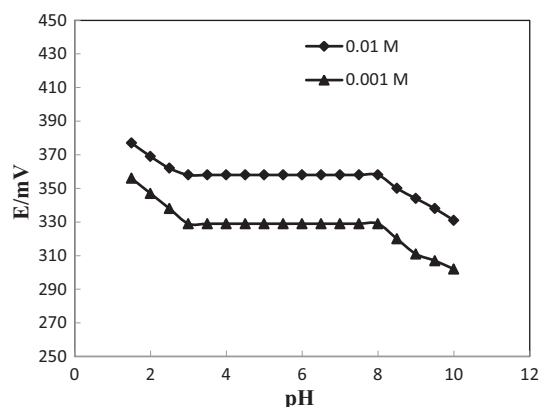


**Fig. 9** pH-potential Profile of Ni(II) membrane sensors at different concentrations.

study entailed the utilization of four variations of plasticizers (*o*-NPOE, DOP, DOPP, and DOS) with HMBT. The impact of various solvent mediators on the membrane response was studied after soaking in a solution of NiCl<sub>2</sub>. The electrode having membrane types 1 yields an expected Nernstian response for Ni<sup>2+</sup>. This is ascertained by comparing the HMBT membrane's calibration curves; one membrane contains *o*-NPOE (type-1), while others contain DOP (type-2), DOPP (type-3), or DOS (type-4). The type-1 membrane's curve has a broader linear range of 10<sup>-7</sup> to 10<sup>-2</sup> M, whereas its Nernstian response was better, which was not the case with other membrane types (Fig. 7, Table 2). The response of electrode with membrane 1 is improved after the utilization of *o*-NOPE.

### 3.4. pH influence on the membrane response

The pH-profile of type-1 membrane is prepared for identifying the electrode's ideal pH range. 10<sup>-3</sup> and 10<sup>-2</sup> M Ni<sup>2+</sup> solutions were used to examine the electrode measurements dependence on pH values. The adjustment of pH was done through the use of 0.1 M hydrochloric acid or 0.1 M sodium hydroxide. As far as type-1 membranes are concerned, the sensor's functional pH range is 3–8 for the two solutions mentioned above (Fig. 9). The nickel ions' hydrolysis caused the curves' breakdown in the typical medium. When the medium is acidic, it is possible to observe an unexpected alteration at pH < 3 for all examined concentrations (10<sup>-3</sup> and 10<sup>-2</sup> M).

### 3.5. Potentiometric selectivity

Selectivity coefficient  $K_{A:B}^{pot}$  elucidates the impact of interfering ions on the sensor's response behavior. Negative data of this coefficient implies that the investigated ion is preferred in relation to the interfering ion. Similarly, positive data means that an electrode is preferred in relation to the interfering ion. Notably, the measurements of selectivity coefficients are predicated on their method as well as activity. In this regard, the IUPAC recommends a couple of methods: separate solution method (SSM) and fixed interference method (FIM). This study utilized the SSM method to measure data of selectivity coefficient. Table 4 summarizes the resultant values. As shown in the table, the log  $K_{Ni:M}^{pot}$  values were negative for all tested

ions. This implies that the ions will not interfere with or disturb the functionality of Ni ion selective membranes.

### 3.6. Comparison of the characteristics of Ni(II) sensor with those of the previously Ni(II) reported sensors

Table 5 shows a comparison of the limits of detection, dynamic ranges, slopes and pH ranges of the proposed sensor also in comparison with previously reported Ni(II) sensors. The proposed sensor's utility is proved with regard to the detection limit, dynamic range, as well as selectivity.

### 3.7. Analytical applications

The titration curve illustrates a sharp inflection point at the titrant volume that corresponds to the end point. The evaluation of Ni(II)-selective membrane was demonstrated and one successfully as an indicator electrode in the titration of Ni(II) ions with EDTA in order to detect nickel ions in solutions of 3–8 pH range. Fig. 10 shows the titration of a 10 ml solution of 1.0 × 10<sup>-2</sup> M of Ni(II) ions against 1.0 × 10<sup>-2</sup> M standard solution of EDTA at a pH of around 5.0. The titration curve's end point is sharp and it is possible to determine the concentration of Ni(II) with good accuracy (1.0 ± 0.1) × 10<sup>-2</sup> M.

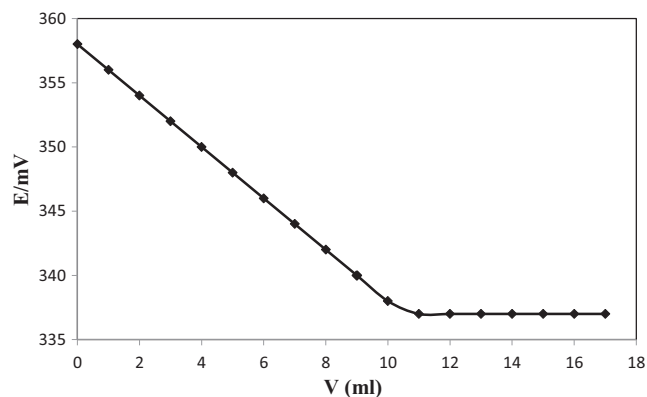
The statistical comparison for the proposed method's data and the conventional volumetric technique (complexometric cyanide ions titration (Suzuki et al., 2003) (Table 6) was made in terms of precision and accuracy. The findings showed a good agreement between the results derived by visual complexometric cyanide ions titration as well as those of the proposed electrode. This does not indicate any major difference between the two methods in terms of either accuracy and precision. At the same time, it is possible to utilize the proposed sensor to analyze Ni<sup>2+</sup> ion in real samples. The proposed method offers the advantages of high accuracy, simplicity, colored solutions, applicability to turbid, low cost, applicable for quality control of ionophore formulations, possible incorporation in automated systems, and rapidity.

**Table 4** Potentiometric selectivity coefficients  $K_{Ni,B}$  of Ni-HMBT -PVC membrane sensor.

Interferent, B	$K_{Ni,B}$
	<i>o</i> -NPOE
Sr <sup>2+</sup>	3.0 × 10 <sup>-3</sup>
Ca <sup>2+</sup>	1.4 × 10 <sup>-3</sup>
Mn <sup>2+</sup>	6.2 × 10 <sup>-3</sup>
La <sup>3+</sup>	2.3 × 10 <sup>-3</sup>
Ba <sup>2+</sup>	1.8 × 10 <sup>-3</sup>
Fe <sup>3+</sup>	2.1 × 10 <sup>-4</sup>
Na <sup>+</sup>	3.5 × 10 <sup>-4</sup>
NH <sub>4</sub> <sup>+</sup>	3.2 × 10 <sup>-3</sup>
K <sup>+</sup>	5.5 × 10 <sup>-4</sup>
Hg <sup>2+</sup>	4.3 × 10 <sup>-4</sup>
Mg <sup>2+</sup>	2.7 × 10 <sup>-4</sup>
Co <sup>2+</sup>	7.3 × 10 <sup>-3</sup>
PO <sub>4</sub> <sup>3-</sup>	6.0 × 10 <sup>-5</sup>
SO <sub>4</sub> <sup>2-</sup>	3.5 × 10 <sup>-5</sup>
Cl <sup>-</sup>	2.0 × 10 <sup>-4</sup>

**Table 5** Comparison of the characteristics of the proposed sensor with those of the previously reported Ni(II) sensors.

Ref.	Dynamic range(M)	LOD(M)	Slope (mV/dec)	Resp-onse time (s)	pH range
[18]	$1.0 \times 10^{-8}$ – $1.0 \times 10^{-2}$	$6.0 \times 10^{-8}$	20.0	15	5.0–8.5
[21]	$1.4 \times 10^{-5}$ – $1.0 \times 10^{-1}$	$2.5 \times 10^{-6}$	28.1	15	2.5–7.4
[21]	$8.9 \times 10^{-5}$ – $1.0 \times 10^{-1}$	$1.0 \times 10^{-5}$	35.4	20	2.5–7.4
[21]	$5.6 \times 10^{-6}$ – $1.0 \times 10^{-1}$	$1.0 \times 10^{-6}$	30.1	20	2.5–7.4
[21]	$7.1 \times 10^{-5}$ – $1.0 \times 10^{-1}$	$1.0 \times 10^{-5}$	37.6	25	2.5–7.4
[19]	$2.0 \times 10^{-7}$ – $1.0 \times 10^{-2}$	$3.2 \times 10^{-6}$	30.0	< 10	4.5–9.0
[20]	$7.9 \times 10^{-6}$ – $1.0 \times 10^{-1}$	$1.0 \times 10^{-6}$	30.0	15	2.7–7.6
[24]	$1.0 \times 10^{-5}$ – $1.0 \times 10^{-1}$	$7.0 \times 10^{-6}$	29.5	< 25	2.6–6.8
This work	$1.0 \times 10^{-8}$ – $1.0 \times 10^{-2}$	$5.0 \times 10^{-8}$	29.3	11	3.0–8.0

**Fig. 10** Potentiometric titration curve of 10.0 ml of a  $1.0 \times 10^{-2}$  M Ni(II) solution, with a  $1.0 \times 10^{-2}$  M EDTA using the proposed membrane sensor as an indicator electrode.**Table 6** Determination of nickel in different water samples using Ni-HMBT-PVC membrane sensor.

Sample	Recovery*, %	
	ISE ( <i>o</i> -NPOE)	EDTA Method [42]
Laboratory water	$100.1 \pm 0.15$	$99.7 \pm 0.12$
Mineral water	$99 \pm 0.27$	$99 \pm 0.23$
Tap water	$98 \pm 0.21$	$98 \pm 0.18$

\* Average of 5 measurements  $\pm$  S.D.**Table 7** Precision and recovery for the determination of ( $1 \times 10^{-4}$  M) Ni(II) in binary mixtures.

Added cation ( $1 \times 10^{-2}$ M)	Recovery (%)*	
	Ni- HMBT -PVC- <i>o</i> -NPOE	
Mg <sup>2+</sup>	98.1	1.3
Ca <sup>2+</sup>	97.2	1.4
Na <sup>+</sup>	98.8	0.2
NH <sup>4+</sup>	98.3	1.2
La <sup>3+</sup>	98.3	0.9
K <sup>+</sup>	99.7	1.2
Ba <sup>2+</sup>	98.2	0.7
Fe <sup>3+</sup>	96.1	1.2
Co <sup>2+</sup>	95.2	1.9
Mn <sup>2+</sup>	93.5	1.7

\* Average of five measurements.

Due to the prudent selectivity of Ni(II) sensor, it was used to directly monitor Ni(II) ions in binary mixtures. Table 7 shows the findings obtained through this procedure. It is evident that the recovery of Ni(II) ions in various binary mixtures is in the range of 92.8–100.5%.

#### 4. Conclusion

This work developed a simple and affordable cost method for the determination of the nickel ion in different water samples, based on a novel prepared ionophore (HMBT) as a sensing carrier in PVC matrix. The investigated sensor has high selectivity and sensitivity, reproducibility, and suitable stability, low limit of detection, wide linear range, and fast response time towards Ni<sup>2+</sup> ion. Simultaneously, the proposed sensor can be successfully applied in the determination of Ni<sup>2+</sup> ion in various water samples and as an indicator electrode in potentiometric titration of Ni(II) ions with EDTA.

In order to derive actionable insights about the reaction that takes place between HMBT ionophore and Ni(II) ions, Ni(II) chelate of HMBT ligand was synthesized and its structure was fully identified. The formed bimetallic Ni(II) complex; HMBT-Ni<sub>2</sub>, was also confirmed to have the following formula: [Ni<sub>2</sub>(HMBT)(H<sub>2</sub>O)<sub>2</sub> Cl<sub>2</sub>]. Meanwhile, square planar architecture of the HMBT-Ni<sub>2</sub> complex was confirmed on the basis of its diamagnetic nature and UV-Vis measurement. Such geometrical arrangement has been reiterated through studies of molecular modeling.

#### Declaration of Competing Interest

The authors declare that they have no known competing financial interests or personal relationships that could have appeared to influence the work reported in this paper.

#### Acknowledgement

The authors would like to thank the Deanship of Scientific Research at Umm Al-Qura University for supporting this work by Grant Code: (20UQU0048DSR).

#### References

Aragay, G., Pons, J., Merkoçi, A., 2011. Recent trends in macro-, micro-, and nanomaterial-based tools and strategies for heavy-metal detection. *Chem. Rev.* 111, 3433–3458.

- Arpa, Ç., Bektas, S., 2006. Preconcentration and determination of lead, cadmium and nickel from water samples using a polyethylene glycol dye immobilized on poly(hydroxyethylmethacrylate) microspheres. *Anal. Sci.* 22, 1025–1029.
- Chen, S., Yan, J., Li, J., Lu, D., 2019. Dispersive micro-solid phase extraction using magnetic ZnFe 2 O 4 nanotubes as adsorbent for preconcentration of Co(II), Ni(II), Mn(II) and Cd(II) followed by ICP-MS determination. *Microchem. J.* 147, 232–238.
- Chohan, Z.H., Sumra, S.H., 2010. Synthesis, characterization and biological studies of oxovanadium (IV) complexes with triazole-derived Schiff bases. *Appl. Organometal. Chem.* 24, 122–130.
- Craggs, A., Moody, G.J., Thomas, J.D.R., 1974. PVC matrix membrane ion-selective electrodes. Construction and laboratory experiments. *J. Chem. Educ.* 51, 541–544.
- Deng, Q.W., Chen, M.H., Kong, L.M., Zhao, X., Guo, J., Wen, X.D., 2013. Novel coupling of surfactant assisted emulsification dispersive liquid–liquid microextraction with spectrophotometric determination for ultra trace nickel. *Spectrochim. Acta Part A* 104, 64–69.
- Dobrowolski, R., Otto, M., 2012. Determination of nickel and cobalt in reference plant materials by carbon slurry sampling GFAAS technique after their simultaneous preconcentration onto modified activated carbon. *J. Food. Compos. Anal.* 26, 58–65.
- Elmosallamy, M.A.F., Saber, A.L., 2016. Recognition and quantification of some monoamines neurotransmitters. *Electroanalysis* 28, 2500–2505.
- Elsherbiny, A.S., El-Ghamry, H.A., 2015. Synthesis, characterization, and catalytic activity of new Cu(II) complexes of Schiff Base: effective catalysts for decolorization of Acid Red 37 dye solution. *Int. J. Chem. Kinet.* 47, 162–173.
- Fan, C., Pan, Q., Li, Q., Wang, L., 2016. Cloud point-TiO<sub>2</sub>/sepiolite composites extraction for simultaneous preconcentration and determination of nickel in green tea and coconut water. *J. Iran. Chem. Soc.* 13, 331–337.
- Gaber, M., Fathalla, S.K., El-Ghamry, H.A., 2019. 2,4-Dihydroxy-5-[(5-mercaptop-1H-1,2,4-triazole-3-yl)diazonyl]benzaldehyde acetato, chloro and nitrate Cu(II) complexes: Synthesis, structural characterization, DNA binding and anticancer and antimicrobial activity. *Appl. Organomet. Chem.* 33, e4707.
- Gómez-Nieto, B., Gismeran, M.J., Sevilla, M.T., Procopio, J.R., 2013. Simultaneous and direct determination of iron and nickel in biological solid samples by high-resolution continuum source graphite furnace atomic absorption spectrometry. *Talanta* 116, 860–865.
- Gupta, V.K., Goyal, R.N., Bachheti, N., 2007. Nickel(II)-selective sensor based on dibenzo-18-crown-6 in PVC matrix. *Talanta* 71, 795–800.
- Gupta, V.K., Jain, A.K., Khurana, U., 1997. Porphyrins as carrier in PVC based membrane potentiometric sensors for nickel(II). *Anal. Chim. Acta* 355, 33–41.
- Gupta, V.K., Prasad, R., Mangla, R., 2000. New nickel(II) selective potentiometric sensor based on 5,7,12,14-tetramethylbenzotetraazaannulene in a poly(vinyl chloride) matrix. *Anal. Chim. Acta* 420, 19–27.
- Gupta, V.K., Singh, A.K., Pal, M.K., 2008. Ni(II) selective sensors based on Schiff bases membranes in poly(vinyl chloride). *Anal. Chim. Acta.* 624, 223–231.
- Huang, Y.L., Tsai, Y.F., Lin, T.H., 1999. Electrothermal atomic absorption spectrometric determination of cobalt and nickel in serum with the deproteinization technique. *Anal. Sci.* 15, 79–82.
- HyperChem, 2007. Release 8.03 for Windows, Molecular modeling system, Hypercube Inc.
- Ibrahim, A.B.M., Farh, M.K., El-Gyar, S.A., El-Gahami, M.A., Fouad, D.M., Silva, F., Santos, I.C., Paulo, A., 2018. Synthesis, structural studies and antimicrobial activities of manganese, nickel and copper complexes of two new tridentate 2-formylpyridine thiosemicarbazone ligands. *Inorg. Chem. Com.* 96, 194–201.
- IUPAC, 2000. Analytical chemistry division, commission on analytical nomenclature. *Pure Appl. Chem.* 72, 1852.
- Jafarigol, E., Ghotli, R.A., Hajipour, A., Pahlevani, H., Salehi, M.B., 2021. Tough dual-network GAMAAX hydrogel for the efficient removal of cadmium and nickel ions in wastewater treatment applications. *J. Ind. Eng. Chem.* 94, 352–360.
- Kundu, S., Biswas, S., Mondal, A.S., Roy, P., Mondal, T.K., 2015. Template synthesis of square-planar Ni(II) complexes with new thiophene appended Schiff base ligands: Characterization, X-ray structure and DFT calculation. *J. Mol. Struct.* 1100, 27–33.
- Leovac, V.M., Jovanovic, L.S., Divjakovic, V., Pevec, Leban, A.I. Armbruster, T., 2007. Transition metal complexes with thiosemicarbazide-based ligands. Part LIV. Nickel(II) complexes with pyridoxal semi- (PLSC) and thiosemicarbazone (PLTSC). Crystal and molecular structure of [Ni(PLSC)(H<sub>2</sub>O)<sub>3</sub>](NO<sub>3</sub>)<sub>2</sub> and [Ni(PLTSC-H)py]NO<sub>3</sub>. *Polyhedron* 26, 49–58.
- Li, L.N., Li, N.B., Luo, H.Q., 2006. A new chemiluminescence method for the determination of nickel ion. *Spectrochim. Acta A* 64, 391–396.
- Martín-Cameán, A., Jos, A., Calleja, A., Gil, F., Iglesias-Linares, A., Solano, E., Cameán, A.M., 2014. Development and validation of an inductively coupled plasma mass spectrometry (ICP-MS) method for the determination of cobalt, chromium, copper and nickel in oral mucosa cells. *Microchem. J.* 114, 73–79.
- Mashhadizadeh, M.H., Momeni, A., 2003. Nickel(II) selective membrane potentiometric sensor using a recently synthesized mercapto compound as neutral carrier. *Talanta* 59, 47–53.
- Mashhadizadeh, M.H., Sheikhshoae, I., Saeid-Nia, S., 2003. Nickel (II)-selective membrane potentiometric sensor using a recently synthesized Schiff base as neutral carrier. *Sens. Actuators B Chem.* 944, 241–246.
- Mattison, R.L., Bowyer, A.A., New, E.J., 2020. Small molecule optical sensors for nickel: The quest for a universal nickel receptor. *Coord. Chem. Rev.* 425, 213522.
- Mazloun, M., Niassary, M.S., Amini, M.K., Pentacyclooctaaza as a neutral carrier in coated-wire ion-selective electrode for nickel(II), *Sens. Actuators B Chem.* 82, 259–264.
- Meeravali, N.N., Kumar, S.J., 2012. Determination of Cd, Pb, Cu, Ni and Mn in effluents and natural waters by a novel salt induced mixed-micelle cloud point extraction using ETAAS. *Anal. Methods* 4, 2435–2440.
- Minami, T., Atsumi, K., Ueda, J., 2003. Determination of cobalt and nickel by graphite-furnace atomic absorption spectrometry after coprecipitation with scandium hydroxide. *Anal. Sci.* 19, 313–315.
- Qiao, X.P., Li, H.L., Zhao, W.Z., Li, D.J., 2012. Spectrophotometric studies and applications for the determination of Ni<sup>2+</sup> in zinc–nickel alloy electrolyte. *Spectrochim. Acta Part A* 95, 576–581.
- Saad, F.A., Elghalban, M.G., El-Metwaly, N.M., El-Ghamry, H.A., Khedr, A.M., 2017. Density functional theory/B3LYP study of nanometric 4-(2,4-dihydroxy-5-formylphen-1-ylazo)-N-(4-methylpyrimidin-2-yl)benzenesulfonamide complexes: Quantitative structure–activity relationship, docking, spectral and biological investigations. *Appl. Organometal. Chem.* 31, e3721.
- Saad, F.A., El-Ghamry, H.A., Kassem, M.A., 2019. Synthesis, structural characterization and DNA binding affinity of new bioactive nano-sized transition metal complexes with sulfathiazole azo dye for therapeutic applications. *Appl. Organometal. Chem.* 33, e4965.
- Saber, A.L., 2010. Novel potentiometric sensors for determination of melatonin and oxomemazine in biological samples and in pharmaceutical formulations. *Electroanal. J.* 22, 2997–3002.
- Saber, A.L., Ahmed, A.I., 2016. Novel ionophore for aluminum ion sensors: synthesis and analytical characterization. *EEE Sens. J.* 116, 5867–5874.
- Saleh, M.B., Hassan, S.S.M., Abdel Gaber, A.A., Abdel Kream, N.A., Novel potentiometric membrane sensor for selective determination of aluminum(III) ions, *Anal. Chim. Acta.* 434, 247–253.

- Sereshti, H., Karimi, M., 2014. Optimized solid phase extraction based on diethyldithiocarbamate-coated Fe<sub>3</sub>O<sub>4</sub> magnetic nanoparticles followed by ICP-OES for determination of Cd(II) and Ni(II) in rice and water samples. *J. Iran. Chem. Soc.* 11, 1129–1136.
- Singh, A.K., Saxena, P., 2007. A PVC-based membrane electrode nickel (II) ions for incorporating a tetraazamacrocyclic as an ionophore. *Sens. Actuators B Chem.* 121, 349–355.
- Sumrra, S.H., Chohan, Z.H., 2013. In vitro antibacterial, antifungal and cytotoxic activities of some triazole Schiff bases and their oxovanadium (IV) complexes. *J. Enz. Inhib. Med. Chem.* 28, 1291–1299.
- Sun, Z., Liang, P., Ding, Q., Cao, J., 2006. Determination of trace nickel in water samples by cloud point extraction preconcentration coupled with graphite furnace atomic absorption spectrometry. *J. Hazard. Mater.* 137, 943–946.
- Suzuki, T., Hioki, A., Kurahashi, M., 2003. Development of a method for estimating an accurate equivalence point in nickel titration of cyanide ions. *Anal. Chim. Acta.* 476, 159–165.
- Welcher, F.J., 1958. *The Analytical Uses of Ethylene Diamine-tetraacetic Acid*. D. Van Noster and Camp. Inc., Princeton, New Jersey, 12.